Published in final edited form as:

Cell Rep. 2017 September 26; 20(13): 3176–3187. doi:10.1016/j.celrep.2017.09.006.

Lymphatic vessels balance viral dissemination and immune activation following cutaneous viral infection

Christopher P. Loo[1,#], **Nicholas A. Nelson**[1,#], **Ryan S. Lane**[1], **Jamie L. Booth**[1], **Sofia C. Loprinzi Hardin**[1], **Archana Thomas**[2], **Mark K. Slifka**[2,3], **Jeffrey C. Nolz**[1,3,4], and **Amanda W. Lund**[1,3,4,*]

[1]Department of Cell, Developmental & Cancer Biology, Oregon Health & Science University, Portland, OR, 97239

[2]Division of Neuroscience, Oregon National Primate Research Center, Oregon Health & Science University, Beaverton, OR 97006

[3]Department of Molecular Microbiology & Immunology, Oregon Health & Science University, Portland, OR, 97239

[4]Knight Cancer Institute, Oregon Health & Science University, Portland, OR, 97239

Summary

Lymphatic vessels lie at the interface between peripheral sites of pathogen entry, adaptive immunity, and the systemic host. Though the paradigm is that their open structure allows for passive flow of infectious particles from peripheral tissues to lymphoid organs, virus applied to skin by scarification does not spread to draining lymph nodes. Using cutaneous infection by scarification we analyzed the effect of viral infection on lymphatic transport and evaluated its role at the host-pathogen interface. We found that in the absence of lymphatic vessels, canonical lymph node-dependent immune induction was impaired, resulting in exacerbated pathology and compensatory, systemic priming. Furthermore, lymphatic vessels decouple fluid and cellular transport, in an interferon-dependent manner, leading to viral sequestration while maintaining dendritic cell transport for immune induction. In conclusion, we found that lymphatic vessels balance immune activation and viral dissemination, and act as an ‘innate-like’ component of tissue host viral defense.

eTOC

[*]Corresponding Author: Amanda W. Lund, Oregon Health & Science University, 3181 SW Sam Jackson Park Rd, RJH 6514 - Mail Code L215, Portland, OR 97239, Phone: (503) 494-1095, lunda@ohsu.edu.
[#]Both authors contributed equally to this manuscript.

Author Contributions

C.P.L. and N.A.N. designed, performed, analyzed, and interpreted experiments. R.S.L., J.L.B., and S.C.L.H. performed experiments. A.T. and M.K.S. performed VACV-specific serum IgG assays. J.C.N. provided reagents, consulted on experimental design and interpretation. A.W.L. conceived, designed, performed, analyzed, and interpreted experiments and wrote the manuscript.

Loo *et al* challenge the prevailing view that lymphatic vessels are passive conduits that flush antigen and pathogens to lymphoid tissue. Rather, the authors demonstrate that lymphatic vessels are a selective and active barrier that efficiently coordinates immune activation while also limiting viral spread and subsequent immune pathology.

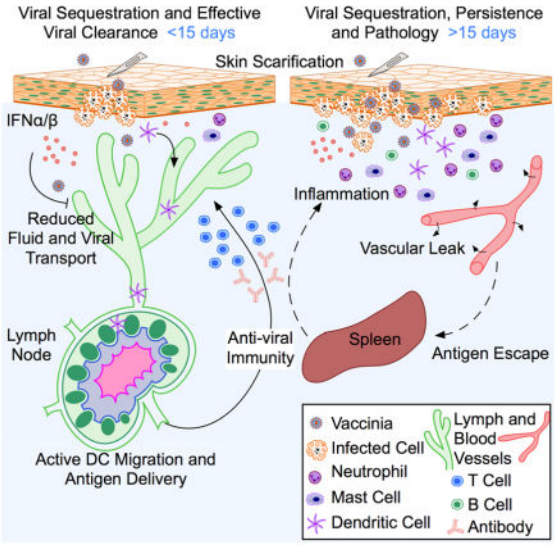

Keywords

lymphatic vessels; cutaneous infection; vaccinia virus; type I interferons; dissemination; tissue microenvironment; tissue immunity

Introduction

Application of the orthopoxvirus vaccinia virus (VACV) to superficially injured skin led to the complete eradication of smallpox (Demkowicz et al., 1996; Hammarlund et al., 2003; Stewart and Devlin, 2006) and motivated investigation into the $CD8^+$ T cell responses that provide protection (Flesch et al., 2010; Moutaftsi et al., 2006; Tscharke et al., 2005, 2006). Despite the role cutaneous tissue damage plays in the efficacy of this vaccine (Liu et al., 2010), very little is known about the associated tissue changes that facilitate the potent, protective immune response. The current immunological paradigm for antigen and viral transport from peripheral tissue indicates that the open structure of lymphatic capillaries allows for rapid, passive propagation of virus and viral antigens to draining lymph nodes (dLN) for presentation to B and T cells (Allan et al., 2006; Bedoui et al., 2009; Carrasco and Batista, 2007; Hickman et al., 2008; Pape et al., 2007). Inconsistent with this paradigm, however, VACV fails to spread to dLNs (Hickman et al., 2013; Khan et al., 2016) and instead remains restricted to the cutaneous site of infection placing a unique requirement on lymphatic vessel function for balancing viral sequestration with active antigen transport and immune induction.

Lymphatic vessels are responsive to their inflamed context (Vigl et al., 2011) and as such pathogen-induced changes in lymphatic vessel transport may influence the host immune

response. Persistent lymphatic vessel hyperplasia results following chronic respiratory tract infection with *mycoplasma pulmonis,* resulting in bronchial lymphedema, and airflow obstruction (Baluk et al., 2005; Yao et al., 2010), and sustained inflammation following *Yersinia pseudotuberculosis* infection induces lymphatic leakage, insufficient dendritic cell (DC) trafficking, and persistently compromised canonical mucosal immunity (Fonseca et al., 2015). Furthermore, corneal herpes simplex 1 (HSV-1) infection induces lymphangiogenesis driven by the expression of vascular endothelial growth factor A (VEGF-A) from infected corneal epithelial cells (Wuest and Carr, 2010), leading to enhanced antigen drainage and $CD8^+$ T cell immunity (Gurung et al., 2016). We therefore hypothesized, that in the context of active viral replication in non-lymphoid tissue, contextual cues influence regional lymphatic vessel function, downstream immune induction, and host viral defense. In the present study, we interrogate the role of the dermal lymphatic vasculature in coordinating both the dissemination of infectious virus and activation of host response to VACV following cutaneous infection.

Results

Cutaneous viral infection induces moderate lymphatic vessel remodeling

Following cutaneous VACV infection innate immune cells infiltrate within and around foci of infected suprabasal keratinocytes while $CXCR3^+CD8^+$ cytotoxic T cells are excluded from lesions but eliminate peripheral infected inflammatory monocytes (Hickman et al., 2013, 2015). The localized and coordinated nature of the host response suggests fine-tuning by soluble and insoluble factors in infected tissue and yet these accompanying tissue changes remain largely unexplored. As such, we sought to evaluate the effect of cutaneous VACV infection on the lymphatic vasculature, a critical interface for the host-pathogen response. Following cutaneous infection with VACV, peak viral titers are detected 3 days post scarification and immune-mediated viral clearance is achieved by day 15 (Khan et al., 2016). Interestingly, VACV results in dermal swelling (Hickman et al., 2013) but unlike multiple models of chronic inflammation and corneal HSV-1 infection (Kim et al., 2014; Wuest and Carr, 2010), neither an increase in lymphatic nor blood vessel density was observed in dermis directly-associated with epidermal hyperproliferation (Figure 1A–E). Rather, dermal lymphatic vessels acquired a more distended, open-lumen morphology (Figure 1C). Confocal imaging confirmed the absence of overt changes in vessel branching (Figure 1F) or increased diameter of lymphatic capillaries (Figure 1G). However, progressive, junctional reorganization of blunt ended lymphatic capillaries was observed, where the normally oak-leaf shaped endothelial cells (Baluk et al., 2007) appeared to elongate resulting in a lengthening of capillary tips and formation of small endothelial sprouts (Figure 1H). Consistent with the limited remodeling observed, vascular endothelial growth factor C (VEGF-C), the primary growth factor driving VEGFR3-dependent lymphangiogenesis, was undetectable in tissue during the first week of infection, whereas levels of VEGF-A (VEGFR1/2 dependent) were elevated (Figure 1I). Further, neither blood (BECs; $CD45^-CD31^+gp38^-$) (Figure 1J) nor lymphatic endothelial cells (LECs; $CD45^-CD31^+gp38^+$) (Figure 1K) demonstrated significant proliferation over sterile infected controls during the first seven days of infection. Conversely, and consistent with stromal reprogramming observed in LNs draining HSV-infected skin (Gregory et al., 2017), LNs

draining VACV-infected tissue demonstrated a greater than 10-fold increase in cell number over the first two weeks of infection (data not shown), accompanied by significant expansion of the nodal lymphatic plexus (Figure 1L).

Importantly, the lack of a lymphangiogenic response in peripheral tissue was not due to direct infection of LECs. Five days following infection with VACV-expressing GFP, we detected GFP^+ actively infected keratinocyte foci and GFP^- foci-associated lymphatic vessels (Suppl. Figure 1A). Furthermore, flow cytometric analysis demonstrated active infection (GFP^+) in $CD45^-CD31^-$ keratinocytes and $CD45^+CD11b^+$ monocytes five days post infection, but not LECs and BECs (Suppl. Figure 1B–F).

Cutaneous viral persistence and pathology in the absence of dermal lymphatic vessels

To specifically evaluate the role of dermal lymphatic vessels in viral control and host-pathogen responses we employed the use of a transgenic mouse where a VEGFR3-Ig fusion protein is expressed under the keratin 14 (K14) promoter (Mäkinen et al., 2001). Transgenic expression of soluble VEGFR3 from basal keratinocytes results in impaired developmental VEGF-C signaling and inhibits maturation of the dermal lymphatic plexus. As a result these mice completely lack a dermal lymphatic vasculature both at steady state (Mäkinen et al., 2001) and during tumor-associated inflammation (Lund et al., 2016). When infected, peak titers were similar between K14 VEGFR3-Ig mice and littermate controls. The absence of dermal lymphatic vessels, however, resulted in significantly delayed viral clearance with elevated viral titers detected in skin 10 days post infection and remaining detectable to day 15 (Figure 2A). No infectious virus was detected in dLNs or ovaries in K14 VEGFR3-Ig mice at days 10 and 25 post infection. Persistent, cutaneous virus was associated with significantly enhanced local pathology characterized by increased ear thickness (Figure 2B), vascular leakiness (Figure 2C), epidermal hyper-proliferation and leukocytic infiltrate (Figure 2D). Elevated levels of infiltrating neutrophils ($Ly6G^+$), B cells ($B220^+$), and degranulating mast cells (toluidine blue stain) were observed in skin of K14 VEGFR3-Ig mice 10 days post infection (Figure 2D), a time point when viral load was not significantly different from littermate controls.

Lymphatic transport is required to generate efficient adaptive immune responses following VACV infection

Given the delay in viral clearance and associated pathology we sought to interrogate the impact of lymphatic transport on adaptive immune responses following VACV infection. In wildtype animals, antigen-specific T cell priming in dLNs results in significant cutaneous infiltration of $CD8^+$ T cells 7 days post infection that continues through day 15 and resolves following viral clearance (Suppl. Figure 2A and B). Reactive germinal centers ($B220^+GL7^+$) are evident in dLNs by day 7 and continue to expand through day 25 (Suppl. Figure 2C). VACV-specific IgG in serum is first detectable at day 7 and increases in concentration through 25 days post infection (Suppl. Figure 2D). Importantly, the kinetics of viral clearance are dependent on the presence of both $CD4^+$ and $CD8^+$ T cells (Suppl. Figure 2E and 2F) consistent with previous reports (Hickman et al., 2013; Xu et al., 2004).

K14 VEGFR3-Ig mice demonstrate impaired fluid transport at steady state (Suppl. Figure 3A) and cellular transport to dLNs following cutaneous challenge with either dibutyl phthalate (Suppl. Figure 3C) or vaccinia (Suppl. Figure 3D), indicating these mice would have an impaired ability to deliver peripherally-restricted antigen for immune priming. Response to systemic challenge, however, remains in tact (Suppl. Figure 4A–E). Evaluation of cutaneous infiltrates 7 days post infection in K14 VEGFR3-Ig mice revealed similar levels of total leukocytes (Figure 3A) but a significant reduction in $CD8^+$ and $CD4^+$ T cells (Figure 3B and C). Longitudinal evaluation of the immunodominant H2-K^b $B8R_{20-27}$-specific $CD8^+$ T cells in blood demonstrated a delay in T cell priming and quantitatively lower numbers of peak expanded T cells (Figure 3D). To specifically demonstrate impaired de novo $CD8^+$ T cell priming in various tissue compartments we transferred 25,000 TCR-tg P14 $CD8^+$ T cells, specific to the class I-restricted H2-D^b-$GP33_{33-41}$ epitope of LCMV, into mice one day prior to infection with VACV expressing GP33 (VACV-GP33). Mice were euthanized 7, 10, and 15 days post infection and expanded P14 $CD8^+$ T cells were quantified in lymphoid and cutaneous tissues. While P14 $CD8^+$ T cells expanded in dLNs of littermates, with peak numbers observed 10 days post infection and contraction through day 15, P14 $CD8^+$ T cells were not detected in dLNs of K14 VEGFR3-Ig mice at any time point (Figure 3E). In littermates, newly primed $CD8^+$ T cells redistributed to and accumulated in spleens and infiltrated infected cutaneous tissue (Figure 3F and G), however, at early time points, K14 VEGFR3-Ig mice lacked systemic and infiltrating cutaneous P14 $CD8^+$ T cells (Figure 3F and G). By day 15, however, detectable populations of P14 $CD8^+$ T cells began accumulating in spleens and infected skin, indicating compensatory, LN-independent priming. Similarly, in the absence of dermal lymphatic vessels, reactive germinal centers are not detected at days 15 and 25 post infection inf dLNs (Figure 3H) and consistently, serum anti-VACV IgG in K14-VEGFR3-Ig mice is undetectable at day 10 when significant levels have accumulated in controls (Figure 3I). As seen with cellular immunity, anti-VACV IgG accumulates in serum by day 15 and persists at similar levels to littermate controls for at least 60 days post infection.

Adaptive immune priming in mice lacking dermal lymphatic vessels occurs outside of draining lymph nodes

The previous observations indicate that adaptive immunity following cutaneous infection in the absence of dermal lymphatic vessels may bypass canonical, LN-dependent activation. We hypothesized that antigen escape into blood, perhaps driven by the observed increase in vascular permeability (Figure 2C), might allow for this non-canonical immune activation. To specifically demonstrate that antigen escape from infected skin lacking dermal lymphatic vessels leads to priming at a site distal to the dLN we utilized TCR-tg P14 $CD8^+$ T cells lacking L-selectin (CD62L). CD62L, normally expressed by both naïve and central memory T cells, is required for binding to peripheral node addressins and homing across high endothelial venules into secondary lymphoid organs (Bruehl et al., 2000). TCR-tg P14 $CD8^+$ T cells (25,000) were transferred one day prior to infection of either littermate or K14 VEGFR3-Ig animals and peripheral expansion followed in blood for 25 days. Wildtype (WT) but not $CD62L^{-/-}$ (LKO) P14 $CD8^+$ T cells expanded in littermate hosts, with peak numbers reached at day 15 (Figure 4A). In K14 VEGFR3-Ig mice, however, both the WT and LKO P14 $CD8^+$ T cells expanded to similar levels (Figure 4B), demonstrating that

$CD8^+$ T cell priming in these mice occurred independent of LN-homing and activation. Importantly, regardless of P14 transfer, the expansion of endogenous H2-K^b $B8R_{20-27}$-specific $CD8^+$ T cells mirrored the response observed in Figure 3 (data not shown). Furthermore, analysis of spleens 10 days post infection, just prior to detection of serum VACV-specific IgG in K14 VEGFR3-Ig mice, revealed the presence of activated germinal centers ($B220^+GL7^+$) in K14 VEGFR3-Ig mice but not littermate controls (Figure 4C), indicating the spleen as a potential site of LN-independent priming. Importantly, when $CD8^+$ T cell immunity was primed outside of dLNs the normally robust conversion to central memory of H2-K^b $B8R_{20-27}$-specific endogenous T cells following scarification was impaired (Figure 4D), indicating a functional difference in memory induction when priming is compartmentalized outside of LNs.

The generation of systemic immunity to LCMV in K14 VEGFR3-Ig mice (Suppl. Figure 4) indicated we could evaluate the protective capacity of a pre-existing memory population in cutaneous tissue lacking dermal lymphatic vessels and therefore the requirement to re-prime memory cells in dLNs. At memory time points following LCMV-Armstrong infection (>40 days post infection) K14 VEGFR3-Ig mice generated equivalent levels of circulating memory as compared to controls, despite slightly reduced peripheral $CD8^+$ T cell numbers (Suppl. Figure 4F–K). To test the protective capacity of this circulating memory population in the absence of LN priming, we infected mice at memory time points with VACV-GP33 by scarification. Three days post infection with VACV-GP33, systemic levels of P14 $CD8^+$ T cells were equivalent (Figure 4E) but re-expansion in dLNs was only observed in littermate controls (Figure 4F), indicating that again in the absence of draining lymphatic vessels, antigen-presentation in LNs is completely impaired. Even without LN re-priming, however, memory endogenous and P14 $CD8^+$ T cells accumulated in skin of K14 VEGFR3-Ig mice 3 days post VACV infection (Figure 4G and H) and significantly controlled viral replication to similar levels as littermate controls (Figure 4I), indicating both that the dermal microenvironment of K14 VEGFR3-Ig mice supports $CD8^+$ T cell infiltration and that while protective immunity does not require LN priming (Nolz and Harty, 2014), the ability to re-prime may lead to boosted infiltrating numbers over time.

Cutaneous viral infection impairs lymphatic fluid transport

Given the requirement for lymphatic transport in efficient viral control and adaptive immune induction, we sought to understand how the virus itself might alter aspects of lymphatic vessel function within cutaneous tissue in wildtype mice. The accumulation of protein rich interstitial fluid leading to tissue swelling is a hallmark of regional inflammation that may result from the combined effects of enhanced vascular leak, altered lymphatic drainage, hyperproliferation, and leuckocytic infiltration. To evaluate lymphatic vessel function we performed fluorescence microlymphangiography with fluorescent dextran (FITC, 155kDa) 1, 4 and 7 days post infection. We saw a marked reduction in the number of lymphatic vessels in infected skin draining fluorescent dextran at each time point assayed (Figure 5A). Furthermore, quantitative analysis of lymphatic transport by extraction of Evans Blue dye in dLNs following intradermal administration demonstrated a progressive reduction in fluid transport over the first 7 days of infection (Figure 5B). This was coincident with increased vascular permeability (Figure 5C).

We hypothesized that reduced lymphatic transport would lead to impaired dLN viral dissemination in this model. To test the role of lymphatic transport in viral dissemination we administered a VEGFR3-specific form of VEGF-C (VEGF-$C_{Cys158Ser}$) that has previously been shown to induce lymphatic vessel hyperplasia and reduce ultraviolet-induced edema (Kajiya et al., 2009). Daily intradermal injections of VEGF-C (100ng, 1μl) resulted in a slightly reduced viral load in infected skin (Figure 5D) and was sufficient to slightly reduce ear thickness at early time points but did not completely reverse the infection-associated swelling (Figure 5E). No changes in epidermal thickness, $CD45^+$ and $F4/80^+$ infiltrates, or $CD31^+$ blood vessel density were observed in treated skin (Suppl. Figure 5). Rather, analysis of infected ears treated with VEGF-$C_{Cys156Ser}$ demonstrated an increase in lymphatic vessel area (Figure 5F), and importantly as a result of these injections, infectious virus normally restricted to cutaneous tissue was detectable in dLNs (Figure 5H). This data supports the hypothesis that reduced lymphatic transport prevents viral dissemination and demonstrates that increased interstitial fluid pressures resulting from injection, interestingly with (VEGFC) or without (PBS) coincident lymphatic vessel remodeling, overcomes the active lymphatic barrier established following infection.

The surprising reduction of fluid transport may result in altered kinetics of soluble antigen delivery to dLNs where T cell priming is known to occur. We evaluated cutaneous endothelial cell populations by flow cytometry to quantify infection-dependent cell surface expression of the adhesion molecules ICAM-1, P-selectin (CD62P), E-selectin (CD62E) and VCAM-1 on BECs and LECs (Figure 6A and B) to quantify endothelial cell viability and response to local context. At time points where fluid transport was significantly reduced, LECs remained viable and displayed a typical inflammation-associated activation phenotype previously reported to facilitate DC transmigration and LN trafficking (Miteva et al., 2010; Teijeira et al., 2014). Levels of the homeostatic chemokine CCL21, required for DC trafficking, were reduced in dLNs three days post infection (Figure 6C). While LN CCL21 expression is driven by multiple factors, this observation is interestingly consistent with the inductive role of fluid flow in CCL21-expression by fibroblastic reticular cells of the LN (Tomei et al., 2009).

During the first four days post infection, migratory DCs ($MHCII^{hi}CD11c^{int}$) accumulated in LNs draining infected skin (Figure 6D). To directly demonstrate active migration from cutaneous tissue we applied FITC (5% in DMSO) to infected skin 24 hours prior to sacrifice at each indicated time point post infection. Approximately 200 FITC-bearing DCs were observed entering dLNs during each 24 hour period of the first 4 days of infection (Figure 6E), consistent with numbers reported for DC trafficking from HSV-1 infected skin (Allan et al., 2006), but significantly less than that induced by the irritant dibutyl phthalate (Figure 6E). As such, DC trafficking from virally infected tissue is maintained during the first four days of infection when lymphatic fluid transport is progressively decreasing.

Interferon-alpha/beta receptor blockade reverses infection-associated lymphatic remodeling and induces viral dissemination

Given that lymphatic vessel integrity remained intact (Figure 1 and 6), we hypothesized that antiviral mechanisms, e.g. type I interferons (IFN-I), may signal to regulate lymphatic vessel

transport and consequent viral sequestration. IFN-I signaling maintains lymphatic vessel integrity in the context of HSV-1-induced corneal lymphangiogenesis (Bryant-Hudson et al., 2013) and thus might impact lymphatic function in our model. We blocked IFN-I signaling through systemic administration of interferon-alpha/beta receptor alpha chain (IFNAR1) blocking antibody (intraperitoneal, 500μg; MAR1-5A3) prior to and during infection. Antibody-mediated blockade of IFNAR1 did not significantly increase viral titers in infected skin (Figure 7A), nor did it impact lymphatic vessel density (Figure 7B and C). Significant changes were observed in the shape of dermal lymphatic vessels, however, where in MAR1-5A3 treated skin vessels adopted a more distended, rounded morphology as compared to isotype treated mice (Figure 7D). Consistent with these changes, confocal analysis of lymphatic capillary blunt ends revealed a loss of infection-induced blunt end remodeling (Figure 7E), with a return to the naive blunt phenotype. Lymphangiography performed 3 days post infection again revealed a pronounced reduction of lymphatic vessel drainage in infected skin as compared to naïve animals but administration of IFNAR1 blocking antibodies appeared to rescue lymphatic drainage in at least some animals (Figure 7F and G). Furthermore, quantification of Evan's blue in dLN following intradermal injection demonstrated an increased delivery of the injected dye to dLN as compared to isotype treated controls (Figure 7H). Given the improvement in lymphatic transport, we evaluated the presence of infectious virus by plaque assay and observed LN spread of virus in the presence of IFNAR1-blockade (Figure 7I). Furthermore, in dLNs of mice treated with IFNAR1 blocking antibodies virally expressed GFP (VACV-GFP) was detectable in the subcapsular sinus, defined by a $LYVE1^+$ lymphatic endothelial cell lining and $CD169^+$ subcapsular macrophages (Figure 7J). These data indicate that when lymphatic transport is restored, virus escapes to dLNs and largely localizes to the subcapsular sinus, as previously reported following subcutaneous injection (Iannacone et al., 2010; Kastenmüller et al., 2012). As such, viral-dependent remodeling of lymphatic transport function may contribute to the dermal sequestration of infectious virus preventing dissemination.

Discussion

The lymphatic vasculature is a critical interface between peripheral (non-lymphoid) pathogenic challenge and host immunity, and likely a bottleneck that can permit or limit dissemination while also providing the necessary route for antigen presentation and adaptive immunity. The prevailing view that lymphatic vessels are passive conduits that flush antigen and pathogens to lymphoid tissue following challenge is modified by our work, which demonstrates that lymphatic vessels respond to anti-viral signals and reduce fluid transport. Our findings reveal a "innate-like" role for lymphatic vessels in the control and coordination of host responses to VACV, indicating that lymphatic vessels provide an important barrier, for restricting viral spread upstream of innate defenses in the LN such as the subcapsular macrophage (Hickman et al., 2008; Junt et al., 2007). Furthermore, we demonstrate in a robust model of cutaneous infection that LN-dependent, canonical T cell activation is absolutely dependent upon functional lymphatic transport but can be overcome in its absence through systemic compensation.

In contrast to the VEGF-A-induced lymphangiogenesis observed following corneal HSV-1 infection (Wuest and Carr, 2010), we did not observe robust lymphatic vessel remodeling or

lymphangiogenesis. Interestingly, VEGF-C, the growth factor required for lymphatic development (Zheng et al., 2014) and classic inducer of pathologic lymphangiogenesis (Skobe et al., 2001), was not detected in infected tissue. The normally avascular cornea, an immune privileged site, may require robust mechanisms of lymphatic vessel ingrowth to induce host response to infection whereas the pre-existing cutaneous lymphatic vasculature is sufficient for this response. Interestingly, angiogenesis may also be antagonized by type I interferons where down regulation of the receptor is necessary for VEGF-induced angiogenesis (Zheng et al., 2011), indicating anti-viral responses may directly limit angiogenic responses in vascularized tissues.

Lymphatic vessels deliver lymph to the subcapsular sinus where large particulate antigens are captured by interfollicular dendritic cells (Hickman et al., 2008) and subcapsular macrophages (Junt et al., 2007) and soluble proteins are filtered into paracortical conduits for sampling by lymphoid resident DCs (Sixt et al., 2005). Current models of lymphatic transport suggest that soluble antigen delivery to dLNs occurs as early as 30 minutes following antigen introduction into peripheral tissue by injection (subcutaneous, intradermal, and intramuscular) (Gonzalez et al., 2010; Hickman et al., 2008; Junt et al., 2007; Kastenmüller et al., 2012). It has therefore been proposed that in the absence of active host defense mechanisms in LNs (Iannacone et al., 2010; Kastenmüller et al., 2012), the open structure of lymphatic vessels and effects of bulk flow would allow for the passive flushing of pathogens into circulation and distant sites. However, lymphatic vessels actively respond to their inflammatory context resulting in altered junctional morphology and activation profiles (Baluk et al., 2005; Vigl et al., 2011). Here we demonstrate that VACV infection, which does not spread to dLNs (Khan et al., 2016), induces remodeling of interendothelial junctions coincident with a rapid reduction in fluid transport dependent on IFN-I.

Antibody-mediated blockade of IFNAR1 induced viral dissemination to dLNs where virus co-localized with the lymphatic lined subcapsular sinus and $CD169^{+}$ subcapsular macrophages as described following subcutaneous injection (Hickman et al., 2008; Junt et al., 2007). The infection-dependent reduction in lymphatic transport, as measured by the dermal lymphatic uptake and delivery Evan's blue to dLNs, was partially reversed by IFNAR1 blockade, indicating that lymphatic vessels actively regulate fluid transport downstream of anti-viral cues in skin and may limit spread of interstitial components such as infectious virus particles. While it is still possible that the detection of virus in dLNs is aided by reduced anti-viral mechanisms following IFNAR blockade, subcapsular macrophages already exhibit low type I IFN responses to allow viral replication, which is essential for antigen presentation and induction of adaptive antiviral immune responses (Honke et al., 2011). Furthermore, the reported observation that virus is immediately detectable in the subcapsular sinus of wildtype animals following injection (Iannacone et al., 2010; Kastenmüller et al., 2012) indicates that subcapsular macrophages are capable of being infected in the presence of type I IFN signaling. Thus, our data demonstrate that changes in lymphatic transport may limit passive viral dissemination to dLN, providing an additional host defense mechanism upstream of important innate barriers previously described (Iannacone et al., 2010; Junt et al., 2007; Kastenmüller et al., 2012).

These results are consistent with the demonstrated requirement for migratory, cross-presenting DCs in the delivery of peripherally restricted antigen (Allan et al., 2006; Bedoui et al., 2009; Roberts et al., 2016), but now indicate that lymphatic vessels may actively limit passive antigen delivery in an IFN-I-dependent manner. Interestingly, in corneal HSV-1 infection, genetic loss of IFNAR1 resulted in reduced lymphatic vessel integrity leading to progressive vessel loss over time (Bryant-Hudson et al., 2013), consistent with our observed role of IFN-I in lymphatic vessel remodeling. Still, in both cases, whether IFN-I directly signals on lymphatic endothelium to mediate these effects or rather acts through an intermediary signal remains to be determined. Taken together, VACV-induced lymphatic vessel remodeling may directly limit pathogen spread while simultaneously promoting induction of an adaptive immune response through active DC transport.

Our work also indicates that lymphatic vessels may be a critical control point for viral manipulation of the host response. While reduction in lymphatic transport may limit viral spread it may also impact the local inflammatory milieu and host response. Saliva from the *Aedes aegypti* mosquitoes, responsible for transmitting arboviruses such as Zika and dengue, induces dramatic local edema leading to viral retention at the bite site and an inflammatory influx of neutrophils that ultimately enhance infection (Pingen et al., 2016). Compartmentalization of infectious virus may regulate balance between local immune pathology, viral persistence, and induction of protective immunity. Consistent with this hypothesis, in the absence of functional dermal lymphatic vessels we decouple viral sequestration from adaptive immunity resulting in profound pathology and viral persistence. We observed elevated infiltration of $Ly6G^+$ cells in mice lacking lymphatic vessels, which demonstrate potent anti-viral activity (Hickman et al., 2013), indicating that neutrophil infiltration or retention may compensate for delayed adaptive immunity to facilitate viral clearance.

Interestingly, prolonged inflammation results in enhanced vascular leakiness that allows for systemic antigen escape and LN-independent priming. Our data indicates that in the absence of lymphatic transport, the host re-compartmentalizes immune induction to compensate for lack of access to the dLNs. Importantly, this compensatory activation must either be dependent upon the robust inflammation induced by viral infection or the potency of viral antigens as similar compensation was not seen in an implanted model of murine melanoma (Lund et al., 2016). This data demonstrates the flexibility of the host immune response but also the impact of altered lymphatic function on the kinetics of regional protective immunity.

Importantly, transgenic mice did not harbor overall immune suppression or increased susceptibility to viral infection and generated long-lived memory following systemic challenge. Memory $CD8^+$ T cells are rapidly recruited to inflamed peripheral tissue in an antigen-independent fashion to provide the first line of defense following re-infection (Ely et al., 2003). Though central memory T cells reacquire expression of CCR7 and CD62L (Sallusto et al., 1999), permitting LN homing, the prevailing hypothesis is that “innate-like” direct recruitment to inflamed tissue may occur in the absence of cognate antigen presentation by DCs in lymphoid tissue (Nolz and Harty, 2014). Our results support this model, where systemic LCMV-specific memory was rapidly recruited to VACV-GP33 infected skin and controlled early replication of virus. The slight reduction in numbers of

P14 TCR-tg $CD8^+$ T cells in infected skin in mice lacking dermal lymphatic vessels, however, may indicate that while re-priming is not necessary for initial recruitment, it does serve to amplify the memory response, leading to more robust antigen-specific memory expansion and recruitment over time.

Tissue microenvironments crucially regulate induction and maintenance of immune responses, compartmentalization of antigen, and accumulation of inflammatory mediators. The data presented herein demonstrate the complexity of the lymphatic vessel response to cutaneous viral challenge and their role in the simultaneous sequestration of infectious virus. Interestingly, it remains to be determined if the virus-induced changes in cutaneous lymphatic vessel function are long-lasting (Yao et al., 2010), and therefore may impact future immunity. In the cornea, inflammation-induced lymphatic vessel regrowth is accelerated following sequential challenge (Kelley et al., 2013), and in lungs the specific sequence of heterologous virus infection determines efficacy of anti-viral immunity and extent of immunopathology (Chen et al., 2003); all together indicating that remodeling of tissue microenvironments can have persistent effects on local immunity with potential clinical implications from host defense to chronic inflammation and immunotherapy.

Experimental Procedures

Mice, in vivo antibodies, and reagents

Specific pathogen-free C57BL/6 mice were obtained from the Jackson Laboratory. K14 VEGFR3-Ig mice (Mäkinen et al., 2001) were a kind gift of Dr. Kari Alitalo and P14 TCR transgenic mice have been previously described (Hogquist et al., 1994; Pircher et al., 1989). L-selectin (CD62L)-deficient mice (Xu et al., 1996) were crossed to P14 TCR-tg and maintained in house. 6–16-week old, male and female mice were used. All animal procedures were approved by and performed in accordance with the IACUC Animal Care and Use Committee. See Supplemental Experimental Procedures for more details.

Viruses and Infections

Mice were infected cutaneously in the ear pinna by 25 pokes with a 29 gauge needle following administration of $5x10^6$ PFU VACV in 10μL PBS to the ventral side of the ear pinna (scarification). See Supplemental Experimental Procedures for more details.

Microlymphangiography and DC Trafficking

Mice were administered 1μL of 1% Evan’s Blue or 10mg/mL 155kD FITC-dextran by injection to the tip of the ear with a Hamilton syringe and imaged with a Zeiss Lumar.V12 Stereo Microscope or iPhone camera. Ears were painted (20μl) with a 5% FITC solution dissolved in 1:1 acetone: dibutyl phalate or acetone:DMSO 24 hours prior to sacrifice.

BrdU Pulse

Mice received 2mg of of BrdU (Sigma-Aldrich) dissolved in 200μL PBS immediately before infection (intraperitoneal), then provided with drinking water containing 0.8mg/mL BrdU for 7 days. See Supplemental Experimental Procedures for more details.

Flow Cytometry

Single cell suspensions were prepared from ears by collagenase IV (5mg/ml) and DNAse (50U/ml) digestion (for endothelial cell extraction) or collagenase D (1mg/ml) and DNAse (50U/ml) (leukocyte extraction) and filtered through 70μm nylon cell strainers. See Supplemental Experimental Procedures for more details.

Anti-VV Serum IgG

Vaccinia specific ELISA was carried out using 96 well micro titer plates coated with vaccinia (WR strain) infected cell lysate. See Supplemental Experimental Procedures for more details. Antibody titers were determined by log-log transformation of the linear portion of the curve using 0.1 optical density as the endpoint and performing conversion of the final values. See Supplemental Experimental Procedures for more details.

Statistics

Statistical significance was calculated by GraphPad (Prism) using parametric or non-parametric Student's *t* tests, one- and two-way ANOVA for multiple pairway testing or Fishers exact test as indicated.

Supplementary Material

Refer to Web version on PubMed Central for supplementary material.

Acknowledgments

The authors would like to thank Drs. Ann B. Hill and David C. Parker for helpful discussion and critical review of the data, Dr. Tim J. Nice for reagents and consultation, Dr. Kari Alitalo for the use of his transgenic mouse model, K14 VEGFR3-Ig, and Tahsin N. Kahn and Jossef F. Osborn for technical support. The authors acknowledge the Knight Cancer Center Flow Cytometry and Advanced Light Microscopy Cores. This work was supported by the OHSU Knight Cancer Center Support grant NIH P30-CA069533 (AWL), Medical Research Foundation of Oregon (AWL), Collins Medical Trust (AWL), U19AI100948 (MKS), and Oregon National Primate Research Center grant, 8P51 OD011092 (MKS). CL and RSL received support from the NIH/NCI Ruth L. Kirchstein National Research Service Award (Molecular Basis of Skin/Mucosa Pathobiology Training Grant; T32-CA106195). AWL is additionally supported by the Department of Defense Peer Reviewed Cancer Research Program (W81XWH-15-1-0348), Cancer Research Institute, V Foundation for Cancer Research (V2015-024) and Melanoma Research Alliance. The authors declare no conflicts of interest.

References

Allan RS, Waithman J, Bedoui S, Jones CM, Villadangos JA, Zhan Y, Lew AM, Shortman K, Heath WR, Carbone FR. Migratory Dendritic Cells Transfer Antigen to a Lymph Node-Resident Dendritic Cell Population for Efficient CTL Priming. Immunity. 2006; 25:153–162. [PubMed: 16860764]

Baluk P, Tammela T, Ator E, Lyubynska N, Achen MG, Hicklin DJ, Jeltsch M, Petrova TV, Pytowski B, Stacker SA, et al. Pathogenesis of persistent lymphatic vessel hyperplasia in chronic airway inflammation. J Clin Invest. 2005; 115:247–257. [PubMed: 15668734]

Baluk P, Fuxe J, Hashizume H, Romano T, Lashnits E, Butz S, Vestweber D, Corada M, Molendini C, Dejana E, et al. Functionally specialized junctions between endothelial cells of lymphatic vessels. J Exp Med. 2007; 204:2349–2362. [PubMed: 17846148]

Bedoui S, Whitney PG, Waithman J, Eidsmo L, Wakim L, Caminschi I, Allan RS, Wojtasiak M, Shortman K, Carbone FR, et al. Cross-presentation of viral and self antigens by skin-derived CD103+ dendritic cells. Nat Immunol. 2009; 10:488–495. [PubMed: 19349986]

Bruehl RE, Bertozzi CR, Rosen SD. Minimal sulfated carbohydrates for recognition by L-selectin and the MECA-79 antibody. J Biol Chem. 2000; 275:32642–32648. [PubMed: 10938267]

Bryant-Hudson KM, Chucair-Elliott AJ, Conrady CD, Cohen A, Zheng M, Carr DJJ. HSV-1 Targets Lymphatic Vessels in the Eye and Draining Lymph Node of Mice Leading to Edema in the Absence of a Functional Type I Interferon Response. Am J Pathol. 2013; 183:1233–1242. [PubMed: 23911821]

Carrasco YR, Batista FD. B Cells Acquire Particulate Antigen in a Macrophage-Rich Area at the Boundary between the Follicle and the Subcapsular Sinus of the Lymph Node. Immunity. 2007; 27:160–171. [PubMed: 17658276]

Chen HD, Fraire AE, Joris I, Welsh RM, Selin LK. Specific History of Heterologous Virus Infections Determines Anti-Viral Immunity and Immunopathology in the Lung. Am J Pathol. 2003; 163:1341–1355. [PubMed: 14507643]

Demkowicz WE, Littaua RA, Wang J, Ennis FA. Human cytotoxic T-cell memory: long-lived responses to vaccinia virus. J Virol. 1996; 70:2627–2631. [PubMed: 8642697]

Ely KH, Cauley LS, Roberts AD, Brennan JW, Cookenham T, Woodland DL. Nonspecific recruitment of memory CD8+ T cells to the lung airways during respiratory virus infections. J Immunol. 2003; 170:1423–1429. [PubMed: 12538703]

Flesch IEA, Woo WP, Wang Y, Panchanathan V, Wong YC, La Gruta NL, Cukalac T, Tscharke DC. Altered CD8 $^{+}$ T Cell Immunodominance after Vaccinia Virus Infection and the Naive Repertoire in Inbred and F $_{1}$ Mice. J Immunol. 2010; 184:45–55. [PubMed: 19949110]

da Fonseca DM, Hand TW, Han SJ, Gerner MY, Zaretsky AG, Byrd AL, Harrison OJ, Ortiz AM, Quinones M, Trinchieri G, et al. Microbiota-Dependent Sequelae of Acute Infection Compromise Tissue-Specific Immunity. Cell. 2015; 163:354–366. [PubMed: 26451485]

Gonzalez SF, Lukacs-Kornek V, Kuligowski MP, Pitcher LA, Degn SE, Kim YA, Cloninger MJ, Martinez-Pomares L, Gordon S, Turley SJ, et al. Capture of influenza by medullary dendritic cells via SIGN-R1 is essential for humoral immunity in draining lymph nodes. Nat Immunol. 2010; 11:427–434. [PubMed: 20305659]

Gregory JL, Walter A, Alexandre YO, Hor JL, Liu R, Ma JZ, Devi S, Tokuda N, Owada Y, Mackay LK, et al. Infection Programs Sustained Lymphoid Stromal Cell Responses and Shapes Lymph Node Remodeling upon Secondary Challenge. Cell Rep. 2017; 18:406–418. [PubMed: 28076785]

Gurung HR, Carr MM, Carr DJJ. Cornea lymphatics drive the CD8+ T-cell response to herpes simplex virus-1. Immunol Cell Biol. 2016

Hammarlund E, Lewis MW, Hansen SG, Strelow LI, Nelson JA, Sexton GJ, Hanifin JM, Slifka MK. Duration of antiviral immunity after smallpox vaccination. Nat Med. 2003; 9:1131–1137. [PubMed: 12925846]

Hickman HD, Takeda K, Skon CN, Murray FR, Hensley SE, Loomis J, Barber GN, Bennink JR, Yewdell JW. Direct priming of antiviral CD8+ T cells in the peripheral interfollicular region of lymph nodes. Nat Immunol. 2008; 9:155–165. [PubMed: 18193049]

Hickman HD, Reynoso GV, Ngudiankama BF, Rubin EJ, Magadán JG, Cush SS, Gibbs J, Molon B, Bronte V, Bennink JR, et al. Anatomically restricted synergistic antiviral activities of innate and adaptive immune cells in the skin. Cell Host Microbe. 2013; 13:155–168. [PubMed: 23414756]

Hickman HD, Reynoso GV, Ngudiankama BF, Cush SS, Gibbs J, Bennink JR, Yewdell JW. CXCR3 Chemokine Receptor Enables Local CD8+ T Cell Migration for the Destruction of Virus-Infected Cells. Immunity. 2015; 42:524–537. [PubMed: 25769612]

Hogquist KA, Jameson SC, Heath WR, Howard JL, Bevan MJ, Carbone FR. T cell receptor antagonist peptides induce positive selection. Cell. 1994; 76:17–27. [PubMed: 8287475]

Honke N, Shaabani N, Cadeddu G, Sorg UR, Zhang DE, Trilling M, Klingel K, Sauter M, Kandolf R, Gailus N, et al. Enforced viral replication activates adaptive immunity and is essential for the control of a cytopathic virus. Nat Immunol. 2011; 13:51–57. [PubMed: 22101728]

Iannacone M, Moseman EA, Tonti E, Bosurgi L, Junt T, Henrickson SE, Whelan SP, Guidotti LG, von Andrian UH. Subcapsular sinus macrophages prevent CNS invasion on peripheral infection with a neurotropic virus. Nature. 2010; 465:1079–1083. [PubMed: 20577213]

Junt T, Moseman EA, Iannacone M, Massberg S, Lang PA, Boes M, Fink K, Henrickson SE, Shayakhmetov DM, Di Paolo NC, et al. Subcapsular sinus macrophages in lymph nodes clear

lymph-borne viruses and present them to antiviral B cells. Nature. 2007; 450:110–114. [PubMed: 17934446]

Kajiya K, Sawane M, Huggenberger R, Detmar M. Activation of the VEGFR-3 pathway by VEGF-C attenuates UVB-induced edema formation and skin inflammation by promoting lymphangiogenesis. J Invest Dermatol. 2009; 129:1292–1298. [PubMed: 19005491]

Kastenmüller W, Torabi-Parizi P, Subramanian N, Lämmermann T, Germain RN. A spatially-organized multicellular innate immune response in lymph nodes limits systemic pathogen spread. Cell. 2012; 150:1235–1248. [PubMed: 22980983]

Kelley PM, Connor AL, Tempero RM. Lymphatic Vessel Memory Stimulated by Recurrent Inflammation. Am J Pathol. 2013; 182:2418–2428. [PubMed: 23578386]

Khan TN, Mooster JL, Kilgore AM, Osborn JF, Nolz JC. Local antigen in nonlymphoid tissue promotes resident memory CD8 $^{+}$ T cell formation during viral infection. J Exp Med. 2016; 213:951–66. [PubMed: 27217536]

Kim H, Kataru RP, Koh GY. Inflammation-associated lymphangiogenesis: a double-edged sword? J Clin Invest. 2014; 124:936–942. [PubMed: 24590279]

Liu L, Zhong Q, Tian T, Dubin K, Athale SK, Kupper TS. Epidermal injury and infection during poxvirus immunization is crucial for the generation of highly protective T cell–mediated immunity. Nat Med. 2010; 16:224–227. [PubMed: 20081864]

Lund AW, Wagner M, Fankhauser M, Steinskog ES, Broggi MA, Spranger S, Gajewski TF, Alitalo K, Eikesdal HP, Wiig H, et al. Lymphatic vessels regulate immune microenvironments in human and murine melanoma. J Clin Invest. 2016

Mäkinen T, Jussila L, Veikkola T, Karpanen T, Kettunen MI, Pulkkanen KJ, Kauppinen R, Jackson DG, Kubo H, Nishikawa S, et al. Inhibition of lymphangiogenesis with resulting lymphedema in transgenic mice expressing soluble VEGF receptor-3. Nat Med. 2001; 7:199–205. [PubMed: 11175851]

Miteva DO, Rutkowski JM, Dixon JB, Kilarski W, Shields JD, Swartz MA. Transmural flow modulates cell and fluid transport functions of lymphatic endothelium. Circ Res. 2010; 106:920–931. [PubMed: 20133901]

Moutaftsi M, Peters B, Pasquetto V, Tscharke DC, Sidney J, Bui HH, Grey H, Sette A. A consensus epitope prediction approach identifies the breadth of murine TCD8+-cell responses to vaccinia virus. Nat Biotechnol. 2006; 24:817–819. [PubMed: 16767078]

Nolz JC, Harty JT. IL-15 regulates memory CD8+ T cell O-glycan synthesis and affects trafficking. J Clin Invest. 2014; 124:1013–1026. [PubMed: 24509081]

Pape KA, Catron DM, Itano AA, Jenkins MK. The Humoral Immune Response Is Initiated in Lymph Nodes by B Cells that Acquire Soluble Antigen Directly in the Follicles. Immunity. 2007; 26:491–502. [PubMed: 17379546]

Pingen M, Bryden SR, Pondeville E, Schnettler E, Kohl A, Merits A, Fazakerley JK, Graham GJ, McKimmie CS. Host Inflammatory Response to Mosquito Bites Enhances the Severity of Arbovirus Infection. Immunity. 2016; 44:1455–1469. [PubMed: 27332734]

Pircher H, Bürki K, Lang R, Hengartner H, Zinkernagel RM. Tolerance induction in double specific T-cell receptor transgenic mice varies with antigen. Nature. 1989; 342:559–561. [PubMed: 2573841]

Roberts EW, Broz ML, Binnewies M, Headley MB, Nelson AE, Wolf DM, Kaisho T, Bogunovic D, Bhardwaj N, Krummel MF. Critical Role for CD103+/CD141+ Dendritic Cells Bearing CCR7 for Tumor Antigen Trafficking and Priming of T Cell Immunity in Melanoma. Cancer Cell. 2016; 30:324–336. [PubMed: 27424807]

Sallusto F, Lenig D, Förster R, Lipp M, Lanzavecchia A. Two subsets of memory T lymphocytes with distinct homing potentials and effector functions. Nature. 1999; 401:708–712. [PubMed: 10537110]

Sixt M, Kanazawa N, Selg M, Samson T, Roos G, Reinhardt DP, Pabst R, Lutz MB, Sorokin L. The conduit system transports soluble antigens from the afferent lymph to resident dendritic cells in the T cell area of the lymph node. Immunity. 2005; 22:19–29. [PubMed: 15664156]

Skobe M, Hawighorst T, Jackson DG, Prevo R, Janes L, Velasco P, Riccardi L, Alitalo K, Claffey K, Detmar M. Induction of tumor lymphangiogenesis by VEGF-C promotes breast cancer metastasis. Nat Med. 2001; 7:192–198. [PubMed: 11175850]

Stewart AJ, Devlin PM. The history of the smallpox vaccine. J Infect. 2006; 52:329–334. [PubMed: 16176833]

Teijeira A, Russo E, Halin C. Taking the lymphatic route: dendritic cell migration to draining lymph nodes. Semin Immunopathol. 2014; 36:261–274. [PubMed: 24402708]

Tomei AA, Siegert S, Britschgi MR, Luther SA, Swartz MA. Fluid Flow Regulates Stromal Cell Organization and CCL21 Expression in a Tissue-Engineered Lymph Node Microenvironment. J Immunol. 2009; 183:4273–4283. [PubMed: 19734211]

Tscharke DC, Karupiah G, Zhou J, Palmore T, Irvine KR, Haeryfar SMM, Williams S, Sidney J, Sette A, Bennink JR, et al. Identification of poxvirus CD8 $^{+}$ T cell determinants to enable rational design and characterization of smallpox vaccines. J Exp Med. 2005; 201:95–104. [PubMed: 15623576]

Tscharke DC, Woo WP, Sakala IG, Sidney J, Sette A, Moss DJ, Bennink JR, Karupiah G, Yewdell JW. Poxvirus CD8+ T-Cell Determinants and Cross-Reactivity in BALB/c Mice. J Virol. 2006; 80:6318–6323. [PubMed: 16775319]

Vigl B, Aebischer D, Nitschké M, Iolyeva M, Röthlin T, Antsiferova O, Halin C. Tissue inflammation modulates gene expression of lymphatic endothelial cells and dendritic cell migration in a stimulus-dependent manner. Blood. 2011; 118:205–215. [PubMed: 21596851]

Wuest TR, Carr DJJ. VEGF-A expression by HSV-1-infected cells drives corneal lymphangiogenesis. J Exp Med. 2010; 207:101–115. [PubMed: 20026662]

Xu J, Grewal IS, Geba GP, Flavell RA. Impaired primary T cell responses in L-selectin-deficient mice. J Exp Med. 1996; 183:589–598. [PubMed: 8627170]

Xu R, Johnson AJ, Liggitt D, Bevan MJ. Cellular and Humoral Immunity against Vaccinia Virus Infection of Mice. J Immunol. 2004; 172:6265–6271. [PubMed: 15128815]

Yao LC, Baluk P, Feng J, McDonald DM. Steroid-resistant lymphatic remodeling in chronically inflamed mouse airways. Am J Pathol. 2010; 176:1525–1541. [PubMed: 20093490]

Zheng H, Qian J, Carbone CJ, Leu NA, Baker DP, Fuchs SY. Vascular endothelial growth factor-induced elimination of the type 1 interferon receptor is required for efficient angiogenesis. Blood. 2011; 118:4003–4006. [PubMed: 21832278]

Zheng W, Aspelund A, Alitalo K. Lymphangiogenic factors, mechanisms, and applications. J Clin Invest. 2014; 124:878–887. [PubMed: 24590272]

Highlights

- Existing, cutaneous lymphatic vessels are sufficient to mediate adaptive immunity.
- Lymphatic vessels are an ‘innate-like’ barrier to cutaneous viral dissemination.
- Skin infection limits fluid but not cellular transport in an IFN dependent manner.
- Lymph node independent immune priming occurs in the absence of lymphatic vessels.

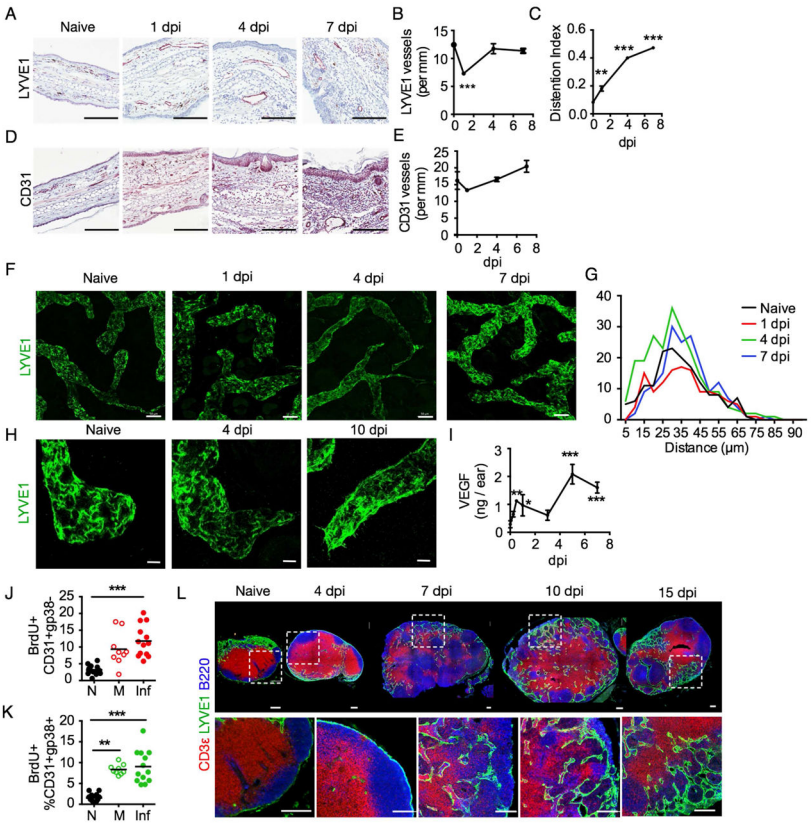

Figure 1. Infection by scarification induces lymphatic vessel remodeling but not lymphangiogenesis

C57Bl/6 mice infected by skin scarification with $2x10^6$ PFU VACV. (A) Representative images of lymphatic vessels (LYVE1) (Scale bar=200μm) and quantification of (B) vessels per length of skin and (C) vessel distension (width/length). (D) Representative images of blood vessels (CD31) (Scale bar=200μm) and (E) quantification of vessels per length of skin. (F) Whole mount images (maximal projection) of skin (scale bar=50μm; LYVE1). (G) Distribution of lymphatic vessel diameters in skin (n=4; >10 measurements per image). (H) Whole mount images (maximal projection) of lymphatic capillary blunt (scale bar=10μm; LYVE1). (I) VEGF-A (pg per ear). (J and K) Mice were infected and pulsed with BrdU (day 0–7) and percent incorporation in (J) blood endothelial cells (BECs;$CD45^-CD31^+gp38^-$) and (K) lymphatic endothelial cells (LECs; $CD45^-CD31^+gp38^+$). Naïve (N) and sterile infected (M) controls. (Each point represents an individual animal). (L) Images of VACV dLNs. (Top) Whole lymph nodes and (Bottom) inset of subcapsular and follicular zones. Lymphatic vessels (LYVE1, green), T cells (CD3ε, red), and B cells (B220, blue). (Scale bar = 200μm.) Statistical significance determined by one-way ANOVA. *p<0.05, **p<0.01, ***p<0.001. See also Figure S1.

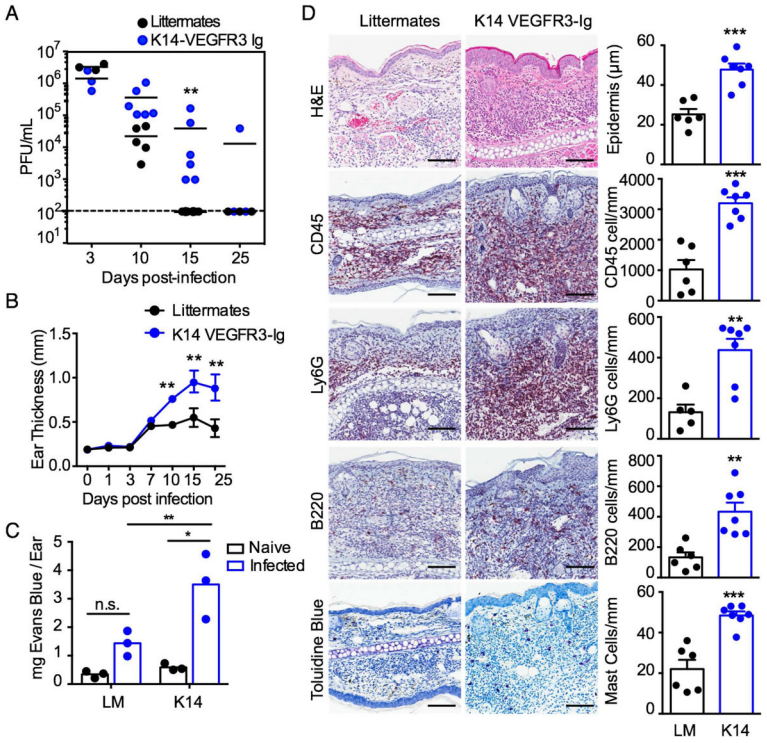

Figure 2. Viral persistence and exacerbated pathology in the absence of lymphatic vessels

K14 VEGFR3-Ig (K14) mice and littermate controls (LM) were infected with VACV by skin scarification. (A) Virus quantified in infected skin (plaque forming units; PFU). (B) Quantification of ear thickness (n>10). (C) Mile's Assay for vascular permeability ten days post infection (dpi) in LM and K14 mice. (D) Tissue histology (representative images; left) and quantification (right) in infected skin 10 dpi. Total leukocytes (CD45), neutrophils (Ly6G), B cells (B220), and degranulating mast cells (toluidine blue). Statistics determined by students unpaired t-test or Fisher's exact test. *p<0.05, **p<0.01, ***p<0.001. Each point represents an individual mouse.

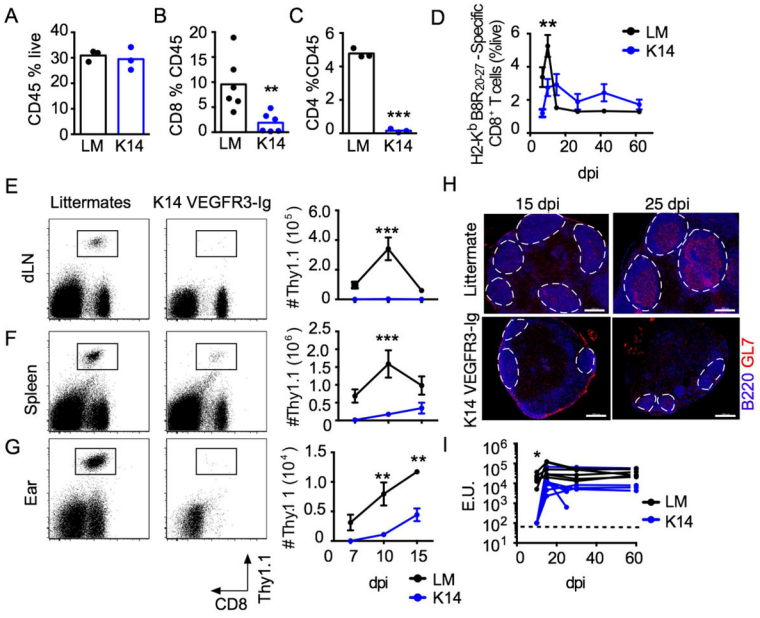

Figure 3. Delayed anti-viral adaptive immune responses in mice lacking dermal lymphatic vessels following scarification

K14 VEGFR3-Ig (K14) mice or littermate controls (LM) were infected by skin scarification with VACV-GP33 (n=4). Quantification of (A) total leukocytes ($CD45^+$ %live) and (B) $CD8^+$ and (C) $CD4^+$ T cells (%CD45) in skin 7 days post infection (dpi). (D) Endogenous H2-K^d $B8R_{20\text{-}27}$-specific CD8+ T cells in blood. (E and F) 25K TCR-tg P14 $Thy1.1^+CD8^+$ T cells transferred in K14 or LM mice one day prior to infection. (E–G) Representative flow plots of $Thy1.1^+CD8^+$ P14 T cells 7 dpi (left; gated on live lymphocytes) and (right) absolute cell numbers on 7, 10 and 15 dpi in (E) draining lymph nodes (dLN), (F) spleen, and (G) infected skin (n≥4). (H) DLNs from K14 VEGFR3-Ig mice and littermate controls imaged by immunofluorescence at 15 and 25 dpi (Scale bar = 200μm, B220, blue; GL7, red). (I) Serum VACV-specific IgG from K14 VEGFR3-Ig mice and littermate controls (Each line is an animal). Dotted line indicates limit of detection. Statistics determined by unpaired students t-test and two-way ANOVA at day 10. *p<0.05, **p<0.01, ***p<0.001. See also Figure S2 and 3.

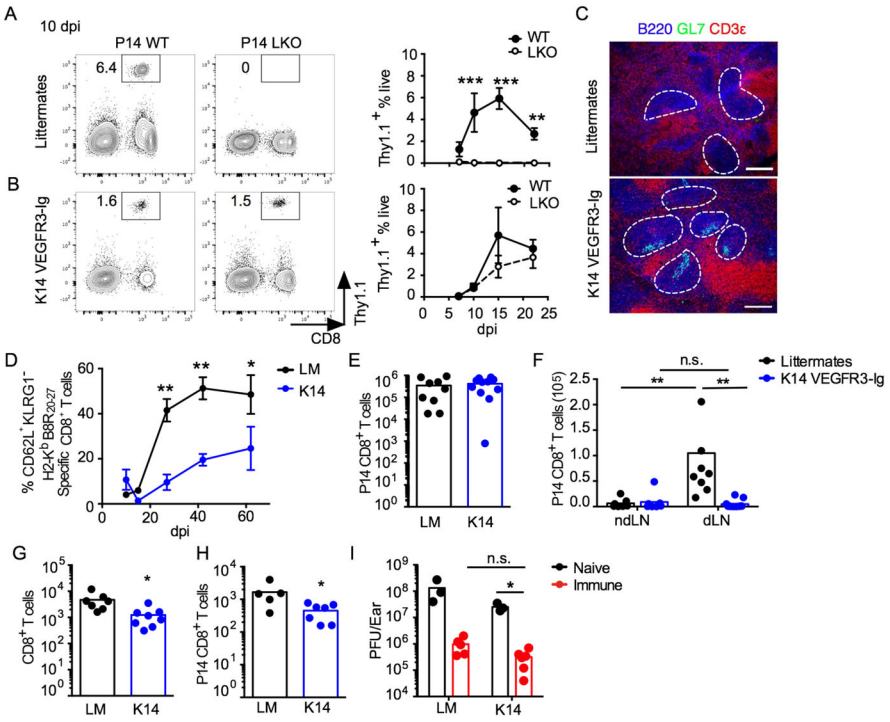

Figure 4. Lymph node independent adaptive immune priming in the absence of dermal lymphatic drainage

Either wildtype (WT) or CD62L knockout (LKO) TCR-tg P14 $CD8^+$ T cells transferred into K14 VEGFR3-Ig (K14) mice or littermate (LM) controls one day prior to infection by scarification with VACV-GP33. (A) Representative plots of circulating $Thy1.1^+$ P14 T cells 10 days post infection (dpi) and (B) quantification in blood ($Thy1.1^+$/live) (n≥4). (C) Spleens from K14 and LM mice evaluated 10 days dpi for reactive germinal centers (Scale bar = 200μm, B220, blue; GL7, green; CD33, red). (D) Acquisition of a central memory phenotype ($CD44^+CD62L^+KLRG1^-$) by circulating H2-K^d $B8R_{20\text{-}27}$-specific endogenous $CD8^+$ T cells in K14 and LM mice. (E–I) LCMV immune mice were infected with VACV-GP33. (E) Number of splenic and (F) lymph node (LN) TCR-tg P14 $CD8^+$ T cells. Number of (G) total endogenous $CD8^+$ T cells or (H) TCR-tg P14 $CD8^+$ T cells in skin 3 dpi. (I) Plaque forming units (PFU) from skin 3 dpi of naïve or LCMV-immune K14 and LM. Data from representative experiment. Statistics determined by unpaired students t-test or one-way ANOVA. *p<0.05, **p<0.01, ***p<0.001. Each point indicates an individual animal. See also Figure S4.

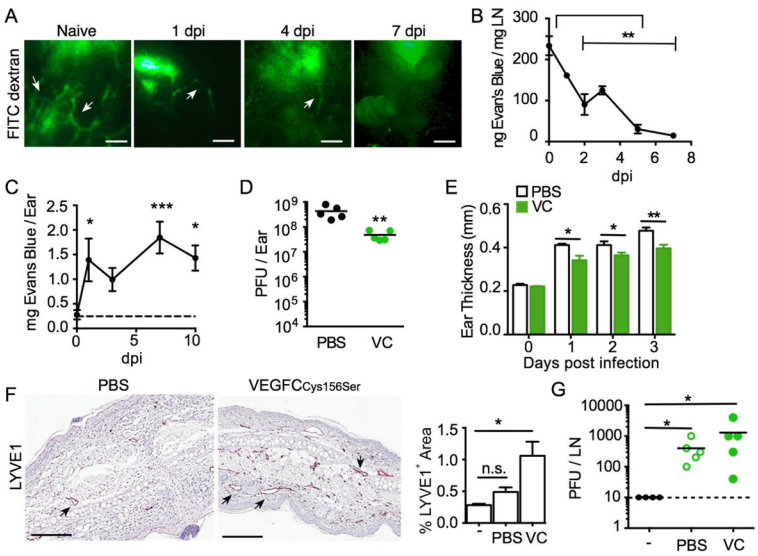

Figure 5. Cutaneous viral infection reduces lymphatic fluid transport

C57Bl/6 mice were infected by skin scarification with VACV. (A) Fluorescence microlymphangiography (155kDa FITC dextran) following scarification (Scale bar=500μm). Arrows indicate draining lymphatic vessels. (B) Quantification of lymphatic drainage following intradermal injection of Evan's Blue and quantification in draining lymph nodes (dLN). (C) Miles' assay for vascular leakiness. (D–I) Intradermal injections of 100ng (1μl) VEGF- C(Cys156Ser) daily starting on the first day of scarification with VACV. (D) Quantification of virus in skin 5 days post infection (dpi) (plaque forming units; PFU). (E) Measurement of ear thickness (n=6). (F) Representative images (left) and quantification (right) of cutaneous lymphatic vessels (purple; LYVE1) following intradermal VEGF-C or PBS (Scale bar=200μm). (I) PFU in dLNs 5 dpi. Statistics determined by one-way ANOVA or Fisher's exact test. *p<0.05, **p<0.01, ***p<0.001. See also Figure S5.

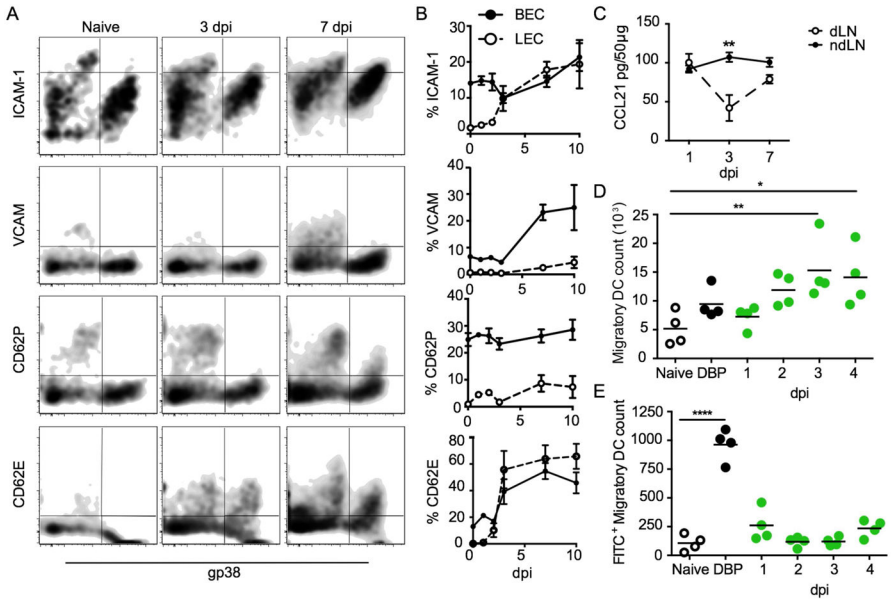

Figure 6. Lymphatic endothelial cells are activated following infection and allow for dendritic cell migration to draining lymph nodes

Wildtype C57BL/6 mice were infected by cutaneous scarification with VACV-GP33. (A) Representative flow cytometry (gated on $CD45^{-}CD31^{+}$) of cutaneous endothelial cells at 0, 3 and 7 days post infection. (B) Quantification of activation markers on blood endothelial cells (BEC; $CD45^{-}CD31^{+}gp38^{-}$) and lymphatic endothelial cells (LEC;$CD45^{-}CD31^{+}gp38^{+}$) (n=6). (C) Quantification of CCL21 in draining lymph nodes (dLN) (n=4). (D) Quantification of migratory DCs present in dLNs following cutaneous VACV infection at the indicated time points or 24 hours following administration of dibutyl phthalate (DBP). (E) Quantification of $FITC^{+}$ migratory DCs present in dLNs. 5% FITC dissolved in DMSO:Acetone painted on skin 24 hours prior to each time point. FITC dissolved in the skin irritant dibutyl phthalate (DBP):acetone used as a positive control. Statistics determined by students unpaired t test. *p<0.05, **p<0.01, ***p<0.001. Each point is an individual mouse.

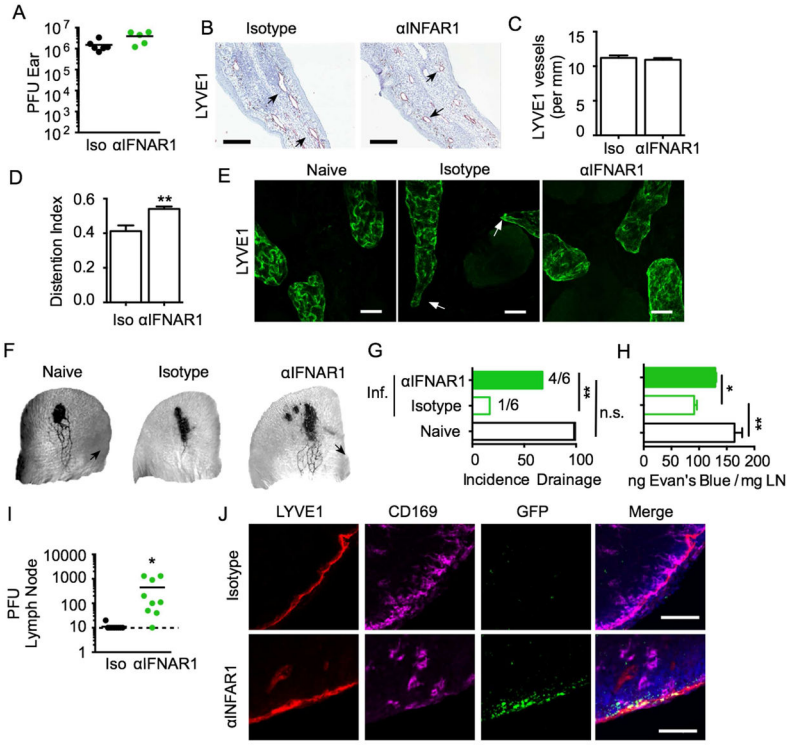

Figure 7. Type I IFN signaling regulates lymphatic remodeling, transport, and viral spread following cutaneous infection

Antibodies blocking the interferon-alpha/beta receptor alpha chain (i.p. 500μg; MAR1-5A3) or isotype control were administered 0 and 2 days post infection (dpi). (A) Quantification of virus in skin 5 dpi (plaque forming unit; PFU). (B) Representative images of lymphatic vessels in infected skin with MAR1-5A3 (αIFNAR1) or isotype control (LYVE1; Scale bar = 200μm). (C) Lymphatic vessel density (vessels per mm length) and (D) lymphatic vessel distension (width/length) (n=7). (E) Whole mount images (maximal projection) of skin 5 dpi (scale bar=50μm; LYVE1, green). (F) Evan's blue lymphangiography (3 dpi). Representative images and (G) incidence of drainage. (H) Quantification of Evan's blue dye in draining lymph nodes (dLN) following intradermal injection (2 dpi). (I) PFU in dLNs (5 dpi). Dotted line indicates limit of detection. (J) Fluorescent imaging of subcapsular GFP in draining lymph nodes 5 dpi with VACV-GFP. (LYVE1, red; CD169, purple; GFP, green; scale bar = 200μm). Statistical significance determined by students unpaired t test or Fishers exact test. *p<0.05, **p<0.01, ***p<0.001. Each point represents an individual animal.